Thermal vacancy formation and $D0_3$ ordering in nanocrystalline intermetallic $(Fe_3Si)_{95}Nb_5$

L. Pasquini*
Institut für Theoretische und Angewandte Physik, Universität Stuttgart, Pfaffenwaldring 57, 70569 Stuttgart, Germany

A. A. Rempel
Institute of Solid State Chemistry, Russian Academy of Sciences, Pervomaiskaya 91, GSP-145, Ekaterinburg 620219, Russia and Institut für Theoretische und Angewandte Physik, Universität Stuttgart, Pfaffenwaldring 57, 70569 Stuttgart, Germany

R. Würschum
Institut für Technische Physik, Technische Universität Graz, Petersgasse 16, A-8010 Graz, Austria and Forschungszentrum Karlsruhe, Institut für Nanotechnologie, Postfach 3640, 76021 Karlsruhe, Germany

K. Reimann and M. A. Müller
Institut für Theoretische und Angewandte Physik, Universität Stuttgart, Pfaffenwaldring 57, 70569 Stuttgart, Germany

B. Fultz
Division of Engineering and Applied Science, 138-78, California Institute of Technology, Pasadena, California 91125

H.-E. Schaefer
Institut für Theoretische und Angewandte Physik, Universität Stuttgart, Pfaffenwaldring 57, 70569 Stuttgart, Germany

(Received 22 September 2000; revised manuscript received 15 December 2000; published 15 March 2001)

The correlation between thermal vacancy characteristics and $D0_3$ ordering in ball-milled nanocrystalline $(Fe_3Si)_{95}Nb_5$ was studied by combined measurements of x-ray diffraction and positron annihilation. Structural stabilization due to grain boundary segregation of Nb enables high-temperature positron lifetime measurements up to 1023 K from which vacancy formation parameters identical to those in single-crystalline $D0_3$ Fe_3Si are deduced. Measurements of coincidence Doppler broadening show that prior to the onset of thermal defect formation in the nanocrystallites, positrons are annihilated in Nb-enriched grain boundaries. The $D0_3$ ordering of the initially disordered Fe_3Si nanocrystallites is discussed on the basis of the thermal vacancy characteristics and self-diffusion behavior.

DOI: 10.1103/PhysRevB.63.134114 PACS number(s): 78.70.Bj, 61.72.Ji, 61.46.+w, 68.35.Ct

I. INTRODUCTION

Many interesting properties of nanocrystalline (*n*-) materials[1] originate with their high number density of interfaces or their mesoscopic crystallites.[2] The high-temperature properties of nanocrystalline materials, in particular their thermal stability, have emerged as important issues. Thermal stability depends on diffusion, and therefore on concentrations and mobilities of point defects. In multicomponent nanocrystalline systems, material properties and thermal stability are further affected by the degree of chemical order within the nanocrystallites. Ordering phenomena in these systems also depend on diffusion and thermal defect formation. Order-disorder phenomena and thermal defect characteristics in nanocrystalline materials affect physical properties, but are also subjects of basic interest within the broader topic of mesoscopic systems with reduced dimensionality.

The present paper reports results from a study of vacancy formation in high temperature thermal equilibrium and the development of $D0_3$ long-range order in initially disordered $(Fe_3Si)_{95}Nb_5$ prepared by mechanical alloying.[3] These studies aim at the correlation between thermal vacancy characteristics and ordering behavior and at the understanding of the microscopic mechanisms underlying the development of chemical order. This goal is achieved using a combination of positron lifetime spectroscopy (PLS) and x-ray diffraction (XRD). PLS is the most appropriate technique to study vacancies in solids[4] owing to the specific sensitivity to free volumes of the positron probe. With a ^{58}Co positron source it is possible to measure the positron lifetime in situ at high temperature and to detect thermal vacancy formation in the bulk and at the interfaces.[5,6]

The Fe-Si-Nb alloy was chosen because it combines, uniquely and conveniently, a high thermal stability and a low vacancy formation enthalpy in $D0_3$-ordered Fe_3Si crystallites. Previous studies in crystallized Finemet showed that a high diffusivity arises from a high thermal vacancy concentration in $Fe_{80}Si_{20}$ nanocrystallites.[5] Here we show that a particular temperature dependence of the mean positron lifetime, displaying a maximum around 800 K, originates from a competition between positron trapping at nanovoids, located in the intersections of crystallite interfaces, and at thermal vacancies in the crystallites. The analysis of this trend within a simple model allows the calculation of the vacancy formation enthalpy in ultrafine grained Fe_3Si crystallites (diameter ca. 100 nm). We also discuss the correlation between chemical ordering and the change in the diffusion behavior resulting from the modification of the local atomic environment.

II. EXPERIMENTAL PROCEDURES

Nanocrystalline powders of $(Fe_3Si)_{95}Nb_5$ were prepared by mechanical attrition with a Spex 8000 laboratory mixer/mill.[3] A mixture of elemental powders with composition 71.25 at. % iron, 23.75 at. % silicon and 5 at. % niobium was sealed under an argon atmosphere in a vial of hard material based on tungsten carbide (HM-WC) with HM-WC balls. The ball-to-powder weight ratio was 4:1 and the powders were milled at room temperature for 48 h. For facilitating the mounting of the positron source the ball-milled powders were compacted at room temperature under uniaxial pressure of 1.5 GPa into disk-shaped pellets.

Positron lifetime spectra were measured by means of $\gamma\gamma$-coincidence and analyzed by numerical standard techniques.[7] For all measurements a ^{58}Co positron source was used depositing $^{58}CoCl_2$ on one side of a specimen with subsequent drying and reduction under a H_2 atmosphere at 483 K for 2 h. The specimen with the ^{58}Co positron source was stacked between identical specimen platelets in a thin-walled Fe container and sealed off in a quartz ampoule under high vacuum. The time resolution of the spectrometer (full width at half maximum) was 215 ps. The number of coincidence counts of most spectra, particularly those measured at high temperature, had to be limited to $0.5-1.0\times10^6$ due to the low count rate associated with the ^{58}Co source. These spectra had to be numerically analyzed with fixed positron lifetime component τ_1.

A series of annealing steps with a holding time of 2 h was carried out *in situ* in the spectrometer, at $T_a=623,713,833$, and 1023 K. Lifetime spectra at ambient temperature were collected following each annealing. PLS measurements at elevated constant temperatures $T<T_a$ were performed after the last three annealing steps.

The evolution of the volume-weighted average grain size $\langle D\rangle_V$, the root-mean-square microstrains $\langle\epsilon^2_{\{hkl\}}\rangle^{1/2}$, the long-range order parameters S_{D0_3},S_{B2} and the lattice parameter a upon annealing was studied by XRD on an equivalent specimen subjected to the same annealing sequence in high vacuum. XRD was performed at room temperature by means of a Siemens D500 diffractometer using Cu-Kα radiation and a secondary graphite monochromator. A Rietveld-like analysis of the x-ray spectra was performed, fitting each Bragg peak profile with two Voigt functions for the $K\alpha_1$ and $K\alpha_2$ lines with the same width. The intensities of these doublets were calculated from the structure factor using the kinematic scattering theory and the appropriate intensity factors.[8] The order parameters S_{D0_3} and S_{B2} were chosen linearly dependent on the site occupancies so that the maximum degrees of order are $S_{D0_3}=1$ and $S_{B2}=1/2$, while the disordered state is characterized by $S_{D0_3}=S_{B2}=0$. Effectively, the dominant contribution to the long range order parameters originated from the ratio of the {111} and {200} superlattice reflections to the fundamental {220} Bragg reflection. Only the $D0_3$ order causes the {111} reflection with an intensity proportional to $S^2_{D0_3}$ whereas the intensity of the {200} reflection depends on $(S_{D0_3}+2S_{B2})^2$ so that one can distinguish between $D0_3$ and $B2$ long-range order. The line widths were fitted to the crystallite size and root mean square microstrains $\langle\epsilon^2_{\{hkl\}}\rangle^{1/2}$ taking into account elastic anisotropy[9] and adding the broadening of the superlattice reflections {111}, {200}, etc. by boundaries of ordered domains.[10]

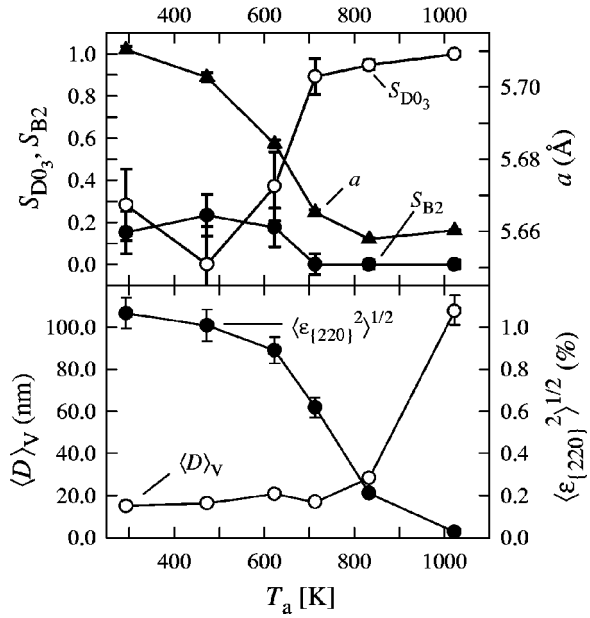

FIG. 1. Long-range order parameters S_{D0_3} and S_{B2}, lattice parameter a, volume-weighted mean grain size $\langle D\rangle_V$, and root mean square microstrain $\langle\epsilon^2_{\{220\}}\rangle^{1/2}$ at ambient temperature after 2 h annealing at T_a. Error bars show the uncertainty due to statistics including correlations between the fitted parameters.

To obtain information on the chemical environment of the atomic free volumes where positrons are annihilated, we measured the electron momentum distribution at the positron annihilation site on a third specimen, both as-prepared and annealed for 2 h at 823 K. These measurements were performed by the coincident Doppler broadening technique at room temperature using a ^{22}Na positron source.[11] Since the thermalized positrons exhibit no momentum, the shift in the energy of the annihilation gamma quanta exclusively originates from the electron momentum distribution. High momenta are due to core electrons. The electron momentum distribution at high momenta is therefore specific and characteristic for the elemental composition at the annihilation site. The coincidence is needed to measure those high momenta almost free of background. To compare electron momentum distributions measured on different specimens, we adopted the following procedure.[11] All the momentum distributions were normalized to unit area. After that, they were divided by the momentum distribution measured with high statistics on a pure Si specimen.

III. RESULTS AND DISCUSSION

A. Ordering and microstructural stability

Figure 1 depicts the variation of the structural parameters, determined by XRD, as a function of the annealing temperature. The as-milled material is characterized by a small grain size $\langle D\rangle_V=15$ nm (in good agreement with previous trans-

TABLE I. Mean positron lifetime $\overline{\tau}$ and component analysis in n-$(Fe_3Si)_{95}Nb_5$ obtained from measurements at ambient temperature after annealing at the temperature T_a. I_1 and I_2 represent the relative intensities of the two components with lifetimes τ_1 and τ_2, respectively.

T_a(K)	$\overline{\tau}$ (ps)	τ_1 (ps)	τ_2 (ps)	I_1 (%)	I_2 (%)
483	222±2	171±1	375±2	75.0±0.5	25.0±0.5
1023	225±2	174±1	370±3	74±1	26±1

mission electron microscopy observations[3]), a high microstrain $\langle \epsilon^2_{\{220\}} \rangle^{1/2} = 1.1\%$ and a very low degree of $D0_3$ long-range order. The lattice parameter of 0.5710 nm is higher than for ordered $Fe_{75}Si_{25}$ ($a = 0.565$ nm, Ref. 12) and even larger than for disordered ball-milled $Fe_{75}Si_{25}$ (0.5663 nm, Ref. 13; 0.5695 nm, Ref. 14). The lattice parameter is also larger than that which is estimated for a disordered solid solution with 25 at. % Si ($a = 0.5699$ nm) by means of extrapolation of the values of a observed for Si contents smaller than 10 at. %.[15] This shows that the enhanced lattice parameter cannot exclusively be attributed to the reduced packing density due to disordering[16] but, additionally, to the partial dissolution of Nb.

After annealing at 483 K for 2 h (the thermal treatment used as the initial state for PLS measurements) a slight decrease is observed in the lattice parameter and in the microstrain $\langle \epsilon^2_{\{220\}} \rangle^{1/2}$, while $\langle D \rangle_V$ is unchanged. The mean positron lifetime $\overline{\tau} = 221 \pm 2$ ps results from the combination of two components with lifetimes $\tau_1 = 171$ ps and $\tau_2 = 375$ ps (Table I). The value of τ_1 is similar to that for monovacancies in α-Fe ($\tau_{1V} = 175$ ps, Ref. 17) and in $D0_3$-Fe_3Si ($\tau_{1V} = 175$ ps, Ref. 18) and therefore characterizes free volumes of the size of one missing atom, while τ_2 is characteristic of nanovoids of the size of 10–15 missing atoms[19] (void diameter 0.5–0.8 nm). Both lifetime components represent a general feature of n-metals.[7,20] The value of τ_1 is ascribed to positron trapping in vacancy-size free volumes in crystallite interfaces or in nonequilibrium vacancies in the crystallites, while τ_2 is associated with nanovoids located at the intersections of the crystallite interfaces. Positron trapping at vacancies in the crystallites probably can be ruled out, first on the basis of the present results derived from coincident Doppler broadening described below. Secondly, previous positron lifetime studies on single-crystalline $D0_3$-Fe_3Si have shown that stoichiometric as well as nonstoichiometric compositions are free of structural vacancies[18] and that nonequilibrium vacancies, which for example are introduced by electron irradiation, anneal out even at ambient temperature.[21]

The absence of a lifetime component smaller than the free lifetime τ_f (Table I) indicates saturation trapping of positrons, which is reasonable because the mean positron diffusion length in metal crystals ($L^+ \approx 100$ nm) is much larger than the grain size and the positrons therefore arrive at the interfacial traps with high probability.

Upon annealing at $T_a = 623$ K, a low degree of long-range order, similar to that in the as-milled state, is present.

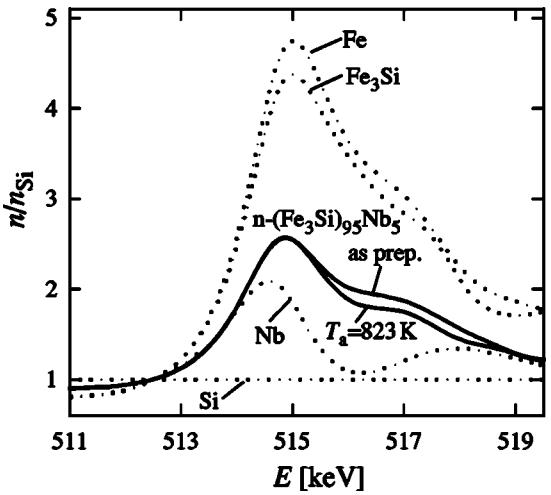

FIG. 2. Coincident Doppler broadening spectra for well-annealed coarse-grained Fe, Fe_3Si, Nb and for n-$(Fe_3Si)_{95}Nb_5$ as-prepared and after annealing at 823 K for 2 h. The spectra are normalized to the spectrum (n_{Si}) of pure defect-free Si. The number n gives the probability of γ quanta with energy E. The spectra were recorded at ambient temperature.

Nearly complete $D0_3$ ordering ($S_{D0_3} \approx 0.9$) is obtained after annealing at 713 K. In the same temperature range initially dissolved Nb atoms segregate at grain boundaries as indicated by Mössbauer spectroscopy.[3,22] The ordering and Nb segregation are accompanied by a further decrease of a (by about 0.9%) and of $\langle \epsilon^2_{\{220\}} \rangle^{1/2}$ (see Fig. 1).

After annealing at the highest temperature ($T_a = 1023$ K), full chemical order is attained and we infer from the sharpness of the {111} superlattice reflections that all antiphase boundaries, in particular those with a displacement vector of $\langle 100 \rangle/2$, are annealed out. The root-mean-square strain $\langle \epsilon^2_{\{220\}} \rangle^{1/2}$ vanishes in this stage, while the lattice parameter a reaches a steady-state value of 0.5658 nm. Assuming that all Nb is segregated to the interfaces, this value corresponds to a composition $Fe_{76}Si_{24}$ (Ref. 13) which is in agreement with the energy-dispersive x-ray analysis.[3] The increased thermal stability of the present alloy to grain growth is attributed to Nb segregation at the interfaces.[3]

Further direct evidence for Nb segregation during ball-milling or subsequent annealing is deduced from the present measurements of the electron momentum distribution by means of coincident Doppler broadening (Fig. 2). These measurements yield information about the chemical environment of free volumes and, for instance, were applied recently for the identification of the different types of vacancies in intermetallic compounds[11] or SiC.[23] The measurements on n-$(Fe_3Si)_{95}Nb_5$ show that the average environment of positron annihilation sites is rich in Nb. Indeed, both the shape and the intensity of the electron momentum distribution at high energies ($E > 518$ keV), which arises from core electrons, nearly coincide with that of Nb and is different from the ones of Fe and Fe_3Si (Fig. 2). The difference in spectra at lower energies comes from changes in the momentum distribution of valence electrons. We emphasize that only the momentum distribution of core electrons is meaningful in rela-

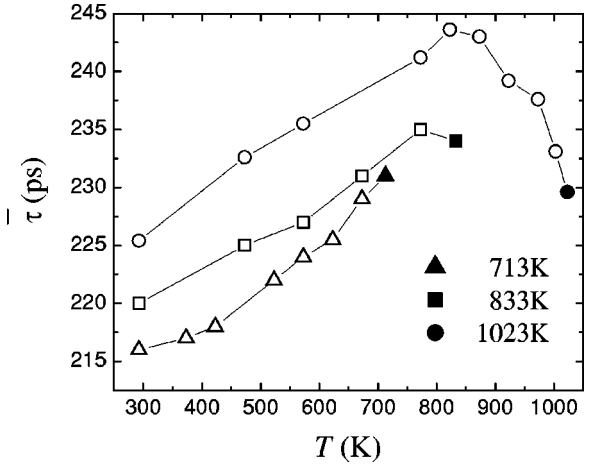

FIG. 3. Mean positron lifetime $\bar{\tau}$ in n-$(Fe_3Si)_{95}Nb_5$ measured in isothermal conditions after (empty symbols) and during annealing (full symbols) at 713, 833, and 1023 K.

tion to the chemical environment of the annihilation site. Based on the results of PLS according to which positron annihilation occurs in the interfaces, this indicates that Nb is segregated to the interfaces. The slight variation upon annealing at 823 K (Fig. 2) indicates the additional Nb segregation which occurs in this temperature regime. These first measurements of a nanocrystalline structure demonstrate that the technique of coincident Doppler broadening is a powerful tool for the study of structural defects in multicomponent disordered media. Indeed, the present result of the segregation of Nb in grain boundaries of n-Fe_3Si is also confirmed by means of a direct analytical imaging technique, i.e., atom-probe field ion microscopy, which was applied for the study of the structurally similar n-alloy $Fe_{73.5}Si_{13.5}B_9Nb_3Cu_1$.[24]

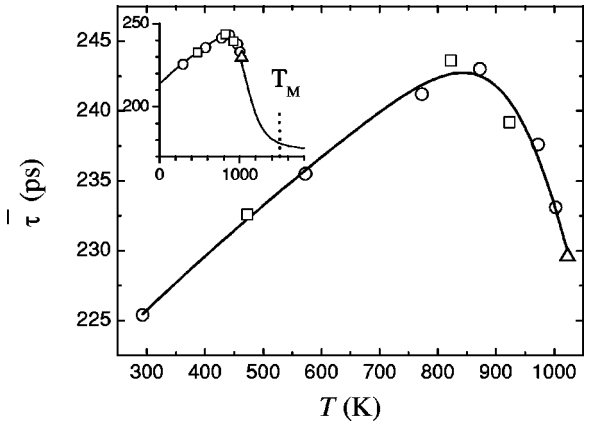

FIG. 4. Mean positron lifetime in n-$(Fe_3Si)_{95}Nb_5$ measured in isothermal conditions with the following sequence: (i) 2 h annealing at $T_a = 1023$ K have been performed (triangle); (ii) the specimen has been cooled down to 293 K and a series of data at increasing temperature up to 1003 K have been measured (circles); (iii) further data have been taken at decreasing temperature (squares). This sequence proves the full reversibility of the observed temperature dependence. The solid line is a fit to the whole set of data according to Eq. (1). The inset shows the same data together with an extension of the fitting curve to higher temperatures.

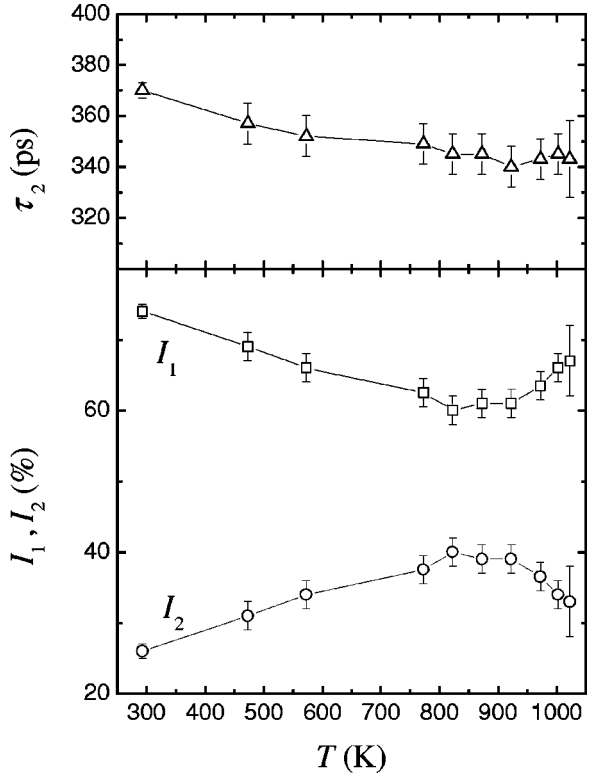

FIG. 5. Two-components analysis: I_1, I_2, τ_2 as a function of temperature in n-$(Fe_3Si)_{95}Nb_5$ annealed at 1023 K. The component τ_1 was fixed to the value of 174 ps derived from the spectrum measured at ambient temperature (see Table I).

B. Thermal vacancy formation

High-temperature positron lifetime measurements on n-$(Fe_3Si)_{95}Nb_5$ were performed after various annealing steps in order to gain insight into thermal defect formation (Fig. 3).

Linear reversible increases of the mean positron lifetime occur after annealing at 713 and 813 K. These changes in lifetime are caused by an increase of the specific positron trapping rate, σ_{void}, of nanovoids, as was found recently[6] for n-$Pd_{84}Zr_{16}$ (see below). Upon further annealing at 1023 K, a decrease of $\bar{\tau}$ occurs above about 820 K. This change in $\bar{\tau}$ is fully reversible as shown by the sequence of data points in Fig. 4. The $\bar{\tau}$-decrease indicates thermal vacancy formation. This unusual signature of positron trapping at thermal vacancies arises from competing positron trapping at nanovoids and vacancy-size free volumes. With increasing temperature, crystal vacancies formed in thermodynamic equilibrium trap positrons with increasing probability. Since the positron lifetime in equilibrium thermal vacancies (τ_V) is similar to that in vacancy-size free volumes at the interfaces (τ_1), the net result of the competitive trapping is the increase in the intensity of the shorter lifetime component τ_1 at the expenses of the nanovoid component (τ_2). This is confirmed by the two-component analysis displayed in Fig. 5. We note that, owing to Nb enrichment at the grain boundaries, a distinction between the vacancy-type interfacial free volumes and the ther-

mal lattice vacancies might be possible by high-temperature measurements of the coincident Doppler broadening.

According to the above interpretation, the temperature dependence of $\overline{\tau}$ can be described by the combination of the temperature behavior of three different traps.

(1) Vacancy-size free volumes at the interfaces with a positron trapping rate independent of temperature, described by[25] $\sigma_1 C_1 = 6\alpha/\langle D\rangle_V$, where α is the trapping coefficient of grain boundaries. With $\alpha = 4.2\times 10^2$ m s^{-1} as determined in Ref. 26 and $\langle D\rangle_V = 110$ nm from XRD analysis, a trapping rate $\sigma_1 C_1 = 2.3\times 10^{10}$ s^{-1} is obtained.

(2) Nanovoids, which have a trapping rate $\sigma_{\rm void} C_{\rm void} = [1+\beta(T-293)](\sigma_{\rm void} C_{\rm void})_{T=293\ {\rm K}}$ that increases linearly with temperature.[6] The value of $(\sigma_{\rm void} C_{\rm void})_{T=293\ {\rm K}}$ can be determined from the intensity ratio $I_2/I_1 = \sigma_{\rm void} C_{\rm void}/\sigma_1 C_1$ (see Ref. 6) measured at $T = 293$ K and the value of $\sigma_1 C_1$ calculated above, giving $(\sigma_{\rm void} C_{\rm void})_{T=293\ {\rm K}} = 0.8 \times 10^{10}$ s^{-1}.

(3) Vacancies in thermodynamic equilibrium, with a specific trapping rate σ_V and a concentration $C_V = \exp(S_V^F/k_B)\exp(-H_V^F/k_B T)$ where H_V^F and S_V^F are the effective vacancy formation enthalpy and entropy, respectively, and k_B is Boltzmann's constant.

In the limit of saturation trapping of positrons, the different types of traps give rise to the trapping-rate averaged mean value of the positron lifetime[6]

$$\overline{\tau} = \frac{\tau_V \sigma_V C_V + \tau_1 \sigma_1 C_1 + \tau_{\rm void}\sigma_{\rm void} C_{\rm void}}{\sigma_V C_V + \sigma_1 C_1 + \sigma_{\rm void} C_{\rm void}}. \qquad (1)$$

Equation (1) with the above values of $\sigma_1 C_1$ and $(\sigma_{\rm void} C_{\rm void})_{T=293\ {\rm K}}$ is used to fit the temperature dependence of the mean positron lifetime after annealing at 1023 K. $\tau_V = \tau_1 = 174$ ps and $\tau_{\rm void} = \tau_2 = 370$ ps, determined by the two-component analysis at ambient temperature (see Table I), are kept constant. The free parameters of the fit are the temperature coefficient β, the preexponential factor $\sigma_V \exp(S_V^F/k_B)$ and the vacancy formation enthalpy H_V^F. The best calculated fit is shown as the continuous line in Fig. 4. For this curve the temperature coefficient of $\sigma_{\rm void}$, associated with the initial linear increase of $\overline{\tau}$, is $\beta = (1.0\pm 0.1)\times 10^{-3}$. A value of $\beta \approx 8\times 10^{-3}$ was determined for neutron irradiated Mo with voids of the size of 2.6 nm (Refs. 6 and 27). In the present case the void diameter is smaller (0.5–0.8 nm). Since the coefficient β is expected to scale linearly with the square of the void diameter,[28] the two results are in fair agreement and confirm that the temperature dependence of $\sigma_{\rm void}$ is the principal reason for the observed linear increase of $\overline{\tau}$ above room temperature.

Table II compares these vacancy formation parameters with those of coarse-grained $D0_3$-ordered $Fe_{79}Si_{21}$ and $Fe_{75}Si_{25}$ (from Ref. 18) and $Fe_{76}Si_{24}$ (from Refs. 29,30). The present value of the vacancy formation enthalpy for n-$(Fe_3Si)_{95}Nb_5$, $H_V^F = 1.1$ eV, is identical with that of other Fe-Si materials. We conclude that the variation of $\overline{\tau}$ at high temperatures can be quantitatively understood on the basis of thermal formation of lattice vacancies. As for $Pd_{84}Zr_{16}$,[6] no indication of additional thermal defect formation in the grain boundaries is found. In both alloys a strong segregation of Zr or Nb at grain boundaries occurs, stabilizing the nanostructure. Since a strong segregation leads to a decrease of the grain-boundary diffusivity,[31] and diffusion is closely linked with thermal defect formation, Zr or Nb segregation may explain the absence of thermal defect formation in grain boundaries in these systems.

TABLE II. Vacancy formation enthalpy H_V^F and preexponential factor $\sigma_V \exp(S_V^F/k_B)$ in n-$(Fe_3Si)_{95}Nb_5$ (this work) and in coarse-grained or monocrystalline $Fe_{75}Si_{25}$, $Fe_{76}Si_{24}$ and $Fe_{79}Si_{21}$.

Material	H_V^F (eV)	$\sigma_V \exp(S_V^F/k_B)$ (10^{16} s^{-1})
n-$(Fe_3Si)_{95}Nb_5$	1.1 ± 0.2	0.5
$Fe_{76}Si_{24}$ (Refs. 29 and 30)	1.06 ± 0.04	2.2 [a]
$Fe_{75}Si_{25}$ (Ref. 18)	0.77 ± 0.08	0.5
$Fe_{79}Si_{21}$ (Ref. 18)	1.11 ± 0.06	4.4

[a] $\sigma_V = 6.6\times 10^{14}$ s^{-1} and $S_V^F = 3.5 k_B$ taken from Refs. 29 and 30, respectively.

The model of competitive positron trapping [Eq. (1)], predicts that the mean positron lifetime decreases further with increasing temperature towards the limiting value τ_V when trapping at thermal vacancies becomes the dominant process. The inset of Fig. 4 shows the fitting function extrapolated to higher temperatures, where the limiting value $\overline{\tau} = \tau_V$ occurs for $T \geqslant 1400$ K (near the melting point, $T_M = 1500$ K). In this temperature regime, however, rapid grain growth might hamper an experimental verification.

C. Correlation between ordering and thermal vacancy characteristics

The thermal vacancy characteristics derived from the positron lifetime studies on n-$(Fe_3Si)_{95}Nb_5$ (Sec. III B) allow a better understanding of the ordering processes which were detected in the present studies by XRD (Sec. III A). Ordering requires the exchange of a substantial fraction of the Si atoms with Fe atoms in a crystallite. We expect these short-range atom movements are mediated by vacancies, as are long-range diffusional movements of atoms. We adopt a simple picture where ordering in the nanocrystallites is completed when all atoms make a few jumps over a distance of an *ordering length* that corresponds to a short diffusion length of typically 1 nm. Since ordering requires diffusion on both sublattices, it is controlled by the species that diffuses more slowly.

The thermal vacancy characteristics are the same in both the $D0_3$-ordered ultrafine grained crystallites (ca. 100 nm diameter) and in coarse-grained material (Table II). Since self-diffusion in Fe_3Si is mediated by vacancies,[21] we may therefore assume that the tracer diffusion characteristics for monocrystalline Fe_3Si also pertain to Fe_3Si nanocrystalllites of $(Fe_3Si)_{95}Nb_5$. The diffusion lengths of either Fe or Si and Ge at 650 K (the mean temperature of the ordering process) were estimated from tracer diffusion data (see Ref. 32) for the disordered ($A2$) and ordered ($D0_3$) materials, and are given in Table III. The diffusion length of Fe in the disor-

TABLE III. Diffusion activation enthalpies Q, frequency factors D_0, and diffusion length $\sqrt{4Dt_a}$ calculated for an annealing time $t_a = 2$ h in different Fe-Si materials.

	Q (eV)	D_0 (m^2/s)	$\sqrt{4Dt_a}$ at 650 K (nm)
^{59}Fe in $D0_3$-$Fe_{76}Si_{24}$ (Ref. 32)	1.64 ± 0.04	$1.3^{+0.5}_{-0.4} \times 10^{-4}$	850
^{71}Ge in $D0_3$-$Fe_{76}Si_{24}$ (Ref. 32)	3.23 ± 0.04	$1.9^{+0.9}_{-0.6} \times 10^{-1}$	0.02 [d]
^{59}Fe in $A2$-$Fe_{76}Si_{24}$	2.2 [a]	8×10^{-4} [a]	14
Si in $A2$-$Fe_{76}Si_{24}$	2.2 [b]	3×10^{-3} [c]	28

[a] Taken from Fig. 14 in Ref. 32 (using the melting temperature of 1500 K of $Fe_{76}Si_{24}$).

[b] Taken from interdiffusion data (Ref. 33) obtained for lower Si concentrations of Fe-Si alloys (8–11 at. % Si). The same value is assumed for the present higher Si concentration since the Si diffusivity hardly depends on the Si concentration (Ref. 33; Fig. 15 in Ref. 32).

[c] Deduced from Fig. 15 of Ref. 32 taking into account the above quoted values of Q (Fe, Si) and D_0 (Fe).

[d] Additional evidence that the Si diffusivity decreases upon ordering is deduced from the decrease of the interdiffusion coefficient at the $A2$-$B2$ ordering transition (Ref. 34) taking into account that Fe diffusivity increases upon ordering (Ref. 32).

dered state exceeds the ordering length of 1 nm and further increases upon the disorder-order transition. This indicates that the ordering is controlled by the diffusion of Si rather than by the diffusion of Fe. In fact, the Si diffusion slows after the disorder-order transition, with the diffusion length of Si (or Ge) in the completely disordered or ordered state being higher or lower than the ordering length, respectively (Table III). An ordering length intermediate between these limiting diffusion lengths is expected because the diffusivity changes upon ordering. In addition to this dependence on ordering, the diffusion that gives rise to ordering might also be affected by residual dissolved Nb.

The correlation of the ordering with the Si diffusion is further supported by Mössbauer studies performed on the same $(Fe_3Si)_{95}Nb_5$ material.[22] These Mössbauer spectrometry studies showed the same temperature range (600–700 K) of ordering as measured in the present XRD studies, and the spectra from samples annealed at high temperatures were consistent with a $D0_3$ long-range order parameter of 0.96. From these previous Mössbauer spectrometry studies, an activation enthalpy of 2.7 eV for $D0_3$ short-range ordering was deduced. Again this value lies between the activation enthalpies of diffusion of Si (or Ge respectively) in the ordered and disordered state (Table III). The activation enthalpy of 2.7 eV along with the preexponential factor of $D_0 = 0.19$ m^2/s of the Si diffusion in $D0_3$-Fe_3Si (Table III), yields a diffusion length of 2.5 nm at 650 K, which is very close to the length required for ordering.

We also note that evidence for ordering processes controlled by the diffusion of Si was found for the Fe_3Si-based nanocrystalline alloy $Fe_{73.5}Si_{13.5}B_9Nb_3Cu_1$ prepared by crystallization.[5]

IV. SUMMARY

The combined use of XRD and PLS was applied to study the ordering and vacancy formation in n-$(Fe_3Si)_{95}Nb_5$ from the disordered as-milled condition to the fully $D0_3$-ordered state with a crystallite size of about 100 nm. $D0_3$ chemical ordering, which occurs upon annealing at 713 K with an activation enthalpy of 2.7 eV, is accompanied by segregation of Nb at the grain boundaries and by a release of internal strains. The kinetics of the ordering is determined by the Si self-diffusivity in the Fe_3Si nanocrystallites which changes with the degree of chemical order. The presence of Nb at the grain boundaries, detected by means of coincidence Doppler broadening, improves the thermal stability sufficiently to allow high-temperature positron lifetime measurements on a stable nanostructure. From these measurements vacancy formation parameters are deduced which are identical to those in single-crystalline $D0_3$-Fe_3Si.

ACKNOWLEDGMENTS

We thank W. Sprengel and M. Eggersmann for helpful discussion and N. Karl for providing the opportunity to perform the x-ray measurements. This work was financially supported by the University of Bologna (L.P.), Max-Planck-Gesellschaft and RFBR Grant No. 99-03-32208a (A.A.R.), Deutsche Forschungsgemeinschaft (Grants Scha428/8-2, 25-1), and European Union (Grant INTAS99-1216).

*Corresponding author. Permanent address: Dipartimento di Fisica, Università di Bologna and Istituto Nazionale per la Fisica della Materia, viale Berti-Pichat 6/2, 40127 Bologna, Italy. E-mail address: pasquini@df.unibo.it

[1] R. Birringer and H. Gleiter, in *Encyclopedia of Materials Science and Engineering*, edited by R. W. Cahn (Pergamon, Oxford, 1988), Suppl. 1, pp. 339–349.

[2] *Nanomaterials: Synthesis, Properties, and Applications*, edited by A.S. Edelstein and R.C. Cammarata (Institute of Physics, Bristol, 1996).

[3] Z. Gao and B. Fultz, Nanostruct. Mater. **2**, 231 (1993).

[4] H.-E. Schaefer, Phys. Status Solidi A **102**, 47 (1987).

[5] R. Würschum, P. Farber, R. Dittmar, P. Scharwaechter, W. Frank, and H.-E. Schaefer, Phys. Rev. Lett. **79**, 4918 (1997).

[6] R. Würschum, E. Shapiro, R. Dittmar, and H.-E. Schaefer, Phys. Rev. B **62**, 12 021 (2000).
[7] H.-E. Schaefer, R. Würschum, R. Birringer, and H. Gleiter, Phys. Rev. B **38**, 9545 (1988).
[8] E. N. Maslen, A. G. Fox, and M. A. O'Keefe, in *International Tables for Crystallography*, edited by A. J. C. Wilson (published for the International Union of Crystallography by Kluwer Academic Publishers, Dordrecht, 1992), Vol. C, Chap. 6.1-2, pp. 476–519.
[9] K. Reimann and R. Würschum, J. Appl. Phys. **81**, 7186 (1997).
[10] B. E. Warren, *X-ray Diffraction* (Addison-Wesley, Reading, MA, 1969).
[11] M.A. Müller, dissertation, University of Stuttgart, 2000.
[12] *Pearsons Handbook of Crystallographic Data for Intermetallic Phases*, Vol. 3, 2nd ed., edited by P. Villars and L. D. Calvart (ASM International Materials Park, OH, 1991).
[13] Y. P. Yelsukov, V. A. Barinov, and G. N. Konygin, Fiz. Met. Metalloved. **62**, 719 (1986) [Phys. Met. Metallogr. **62**, 85 (1986)].
[14] M. Abdellaoui, C. Djega-Mariadassou, and E. Gaffet, J. Appl. Crystallogr. **259**, 241 (1997).
[15] M. Polcarová, K. Godwod, J. Bak-Misiuk, S. Kadecová, and J. Brádler, Phys. Status Solidi A **106**, 17 (1988).
[16] R. W. Cahn, Nature (London) **397**, 656 (1999).
[17] A. Vehanen, P. Hautojärvi, P. Johannson, J. Yli-Kauppila, and P. Moser, Phys. Rev. B **25**, 762 (1982).
[18] E.A. Kümmerle, K. Badura, B. Sepiol, H. Mehrer, and H.-E. Schaefer, Phys. Rev. B **52**, R6947 (1995).
[19] M.J. Puska and R.M. Nieminen, J. Phys. F: Met. Phys. **13**, 333 (1983).
[20] R. Würschum and H.-E. Schaefer, in *Nanomaterials: Synthesis, Properties, and Applications* (Ref. 2), p. 277.
[21] H.-E. Schaefer, K. Frenner, and R. Würschum, Intermetallics **7**, 277 (1999).
[22] Z. Gao and B. Fultz, Nanostruct. Mater. **4**, 939 (1994).
[23] M.A. Müller, A.A. Rempel, K. Reichle, W. Sprengel, J. Major, and H.-E. Schaefer (unpublished).
[24] K. Hono, Acta Mater. **47**, 3127 (1999).
[25] R. Würschum and A. Seeger, Philos. Mag. A **73**, 1489 (1996).
[26] E. Shapiro, R. Würschum, H.-E. Schaefer, H. Ehrhardt, C.E. Krill, and R. Birringer, Mater. Sci. Forum **343-346**, 726 (2000); J. Metastable Nanocryst. Mater. **8**, 726 (2000).
[27] M.D. Bentzon and J.H. Evans, J. Phys.: Condens. Matter **2**, 10 165 (1990).
[28] R.M. Nieminen, J. Laakkonen, P. Hautojärvi, and A. Vehanen, Phys. Rev. B **19**, 1397 (1979).
[29] A. Broska, J. Wolff, M. Franz, and Th. Hehenkamp, Intermetallics **7**, 259 (1999).
[30] R. Kerl, J. Wolff, and Th. Hehenkamp, Intermetallics **7**, 301 (1999).
[31] J. Bernardini, P. Gas, E. D. Hondros, and M. P. Seah, Proc. R. Soc. London, Ser. A **379**, 159 (1982).
[32] A. Gude and H. Mehrer, Philos. Mag. A **76**, 1 (1997).
[33] H.V. Mirani and P. Maaskant, Phys. Status Solidi A **14**, 521 (1972).
[34] E. Rabkin, B. Straumal, V. Semenov, W. Gust, and B. Predel, Acta Metall. Mater. **43**, 3075 (1995).